Supporting Information for:

Actinide complexes with Wells-Dawson Polyoxometalates (Part 2): Californium

Ian Colliard* and Gauthier J.-P. Deblonde*

Lawrence Livermore National Laboratory, Livermore, California 94550, USA

*Colliard1@LLNL.gov ; Deblonde1@LLNL.gov

Table S1. Compilation of californium coordination compounds that have been synthesized and structurally characterized via, at least, single crystal X-ray diffraction.

	Year	Ligand	Compound	Californium coordination number and bonds	Ref
#1	2006	Iodate	$Cf(IO_3)_3$	9 (Cf^{III}-O bonds)	[1]
#2	2010	Aqua-triflate	$[Cf(H_2O)_9](CF_3SO_3)_3$	9 (Cf^{III}-O bonds)	[2]
#3	2014	Borate	$Cf[B_6O_8(OH)_5]$	8 (Cf^{III}-O bonds)	[3]
#4	2015	Dipicolinate	$Cf_2(HDPA)_6 \cdot 2H_2O$	9 (6 Cf^{III}-O + 3 Cf^{III}-N bonds)	[4]
#5	2018	Dithio-carbamates	$Cf(S_2CNEt_2)_3(N_2C_{12}H_8) \cdot CH_3CN$	8 (6 Cf^{III}-S + 2 Cf^{III}-N bonds)	[5]
#6	2019	DOPO[a]	$Cf(DOPO)_3$	9 (6 Cf^{III}-O + 3 Cf^{III}-N bonds)	[6]
#7	2020	Mellitate	$Cf_2(Mellitate)(H_2O)_{10} \cdot 4H_2O$	9 (Cf^{III}-O bonds)	[7]
#8	2020	Squarate	$Cf_2(C_4O_4)_3(H_2O)_4$	9 (Cf^{III}-O bonds)	[8]
#9	2020	Squarate-oxalate	$Cf_2(C_4O_4)_2(C_2O_4)(H_2O)_4$	9 (Cf^{III}-O bonds)	[8]
#10	2021	Metallocene	$Cf(Cp^{tet})_2Cl_2K(OEt_2)$[b]	2 Cp^{tet} ligands + 2 Cf^{III}-Cl bonds.	[9]
#11	2023	Crown-ether	$Cf(18\text{-crown-}6)I_2$	Cf(II) compound. 8 (6 Cf^{II}-O + 2 Cf^{II}-I bonds)	[10]
#12	2024	Pmtz[c]	$[(Cf(pmtz)_2(H_2O)_3)_2(\mu\text{-}pmtz)]_2\text{-}(pmtz)_2 \cdot nH_2O$	9 (6 Cf^{III}-N + 3 Cf^{III}-O bonds)	[11]
#13	This work	Wells-Dawson polyoxometalate	$K_{17}Cf(P_2W_{17}O_{61})_2 \cdot 2H_2O$	8 (Cf^{III}-O bonds)	This work

a: DOPO = 2,4,6,8-tetra-*tert*-butyl-1-oxo-1*H*-phenoxazin-9-olate.
b: Cptet = {C5Me4H}.
c: Pmtz = 5-(pyrimidyl)tetrazolate.

Table S2. Crystallographic table for $Cf^{III}(P_2W_{17})_2$ and $Pr^{III}(P_2W_{17})_2$.

Identification code	cfp2w17_mp	PrWD-K_aP
Empirical formula	$Cf_4K_{68}O_{492}P_{16}W_{136}$	$K_{17}O_{125}P_4PrW_{34}$
Formula weight	37033.92	9180.39
CCDC	2514979	2514973
Temperature/K	298	293(2)
Crystal system	monoclinic	triclinic
Space group	$P2_1/n$	P-1
a/Å	12.3745(2)	14.6606(2)
b/Å	23.4607(3)	22.5777(3)
c/Å	51.8190(6)	24.8922(4)
α/°	90	95.4460(10)
β/°	90.6350(10)	102.7470(10)
γ/°	90	99.3290(10)
Volume/Å^3	15042.9(4)	7856.6(2)
Z	1	2
ρ_{calc}g/cm^3	4.088	3.881
μ/mm^{-1}	27.037	25.656
F(000)	15924.0	7916
Crystal size/mm^3	0.62 × 0.063 × 0.05	0.53 × 0.16 × 0.12
Radiation	Mo Kα (λ = 0.71073)	Mo Kα (λ = 0.71073)
2Θ range for data collection/°	6.586 to 69.668	6.718 to 69.834
Index ranges	-19 ≤ h ≤ 17, -35 ≤ k ≤ 36, -80 ≤ l ≤ 82	-23 ≤ h ≤ 23, -36 ≤ k ≤ 32, -38 ≤ l ≤ 39
Reflections collected	208996	191864
Independent reflections	57285 [R_{int} = 0.1342, R_{sigma} = 0.1074]	58903 [R_{int} = 0.0972, R_{sigma} = 0.0902]
Data/restraints/parameters	57285/0/1652	58903/0/1646
Goodness-of-fit on F^2	1.040	1.036
Final R indexes [I>=2σ (I)]	R_1 = 0.0794, wR_2 = 0.2139	R_1 = 0.0695, wR_2 = 0.2021
Final R indexes [all data]	R_1 = 0.1238, wR_2 = 0.2351	R_1 = 0.0915, wR_2 = 0.2160
Largest diff. peak/hole / e Å^{-3}	4.76/-3.81	6.24/-5.23

Table S3. Select bond list for $Cf(P_2W_{17}O_{61})_2$. The continuous symmetry operation measure (CSoM values) were calculated using the theoretical framework defined by Nielsen & Sørensen.[12] Bond distance and uncertainty values are given in Å.

$K_{17}Cf(P_2W_{17}O_{61})_2 \cdot 2H_2O$ (Monoclinic)		
Cf1	O41	2.430
Cf1	O48	2.465
Cf1	O51	2.383
Cf1	O58	2.362
Cf1	O80	2.434
Cf1	O84	2.468
Cf1	O101	2.479
Cf1	O102	2.392
Average		**2.427**
Uncertainty		**0.012**
CSOM		**0.401**

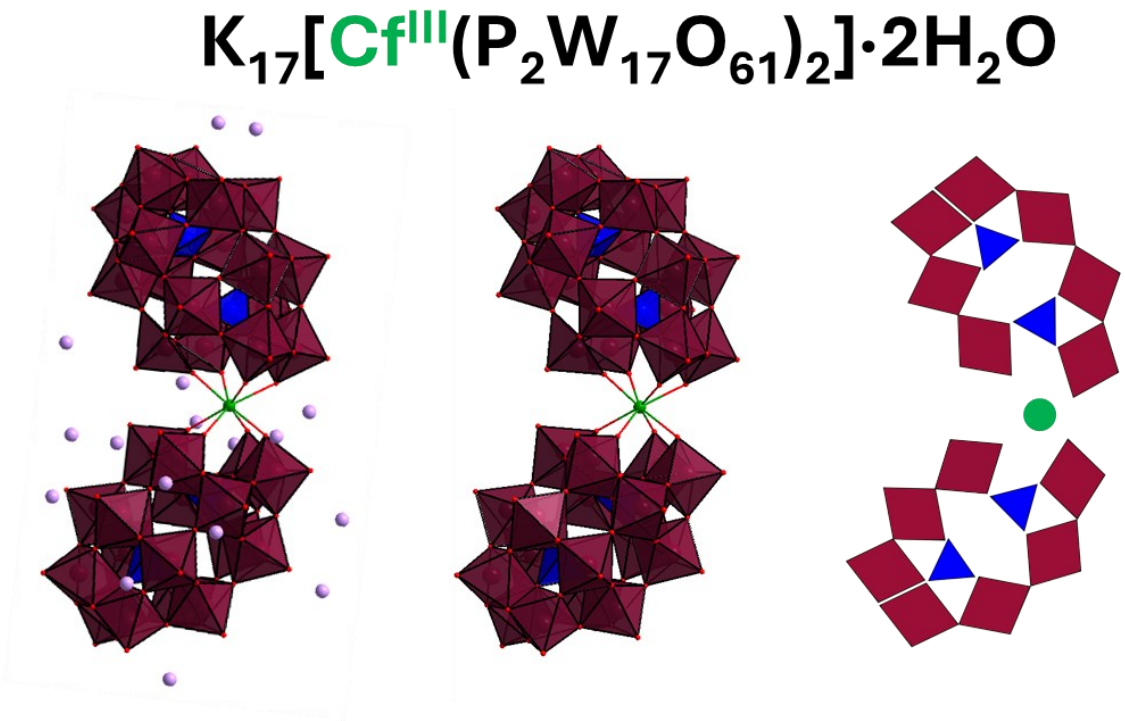

Figure S1. View of the structure of the $[Cf(P_2W_{17}O_{61})_2]^{17-}$ complex. From left to right, complex with its K^+ counterions, complex without counterion, and projection. Green: Cf. Blue: P. Marron: W. Red: O. Purple: K.

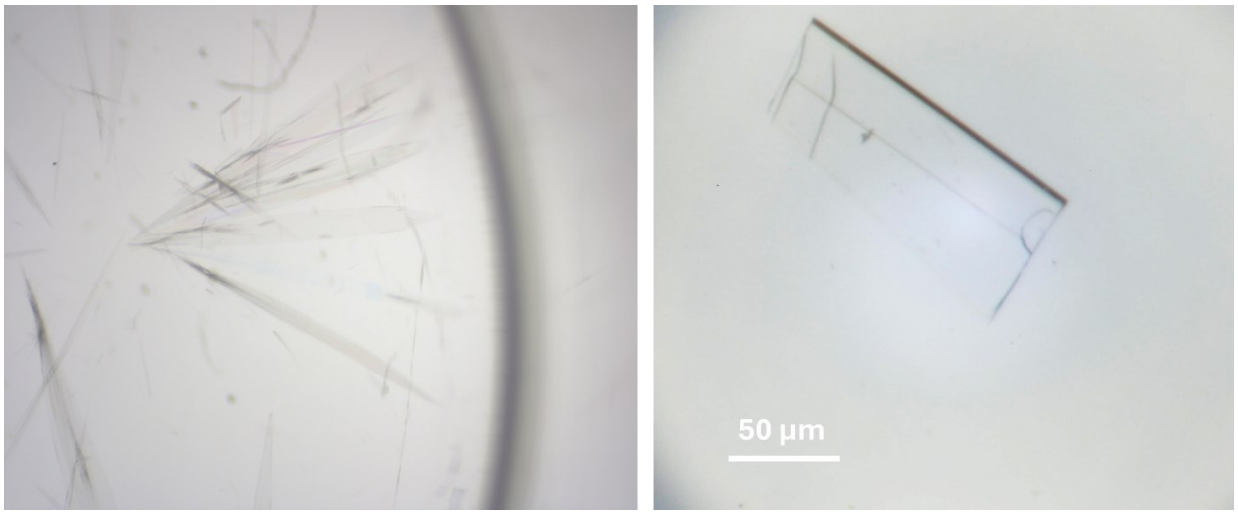

Figure S2. Microscope photographs of $K_{17}Cf(P_2W_{17}O_{61})_2 \cdot 2H_2O$. The crystal morphology is similar to that of the monoclinic phases of $K_{17}Am(P_2W_{17}O_{61})_2 \cdot 12H_2O$ and $K_{17}Cm(P_2W_{17}O_{61})_2 \cdot 8H_2O$.[13]

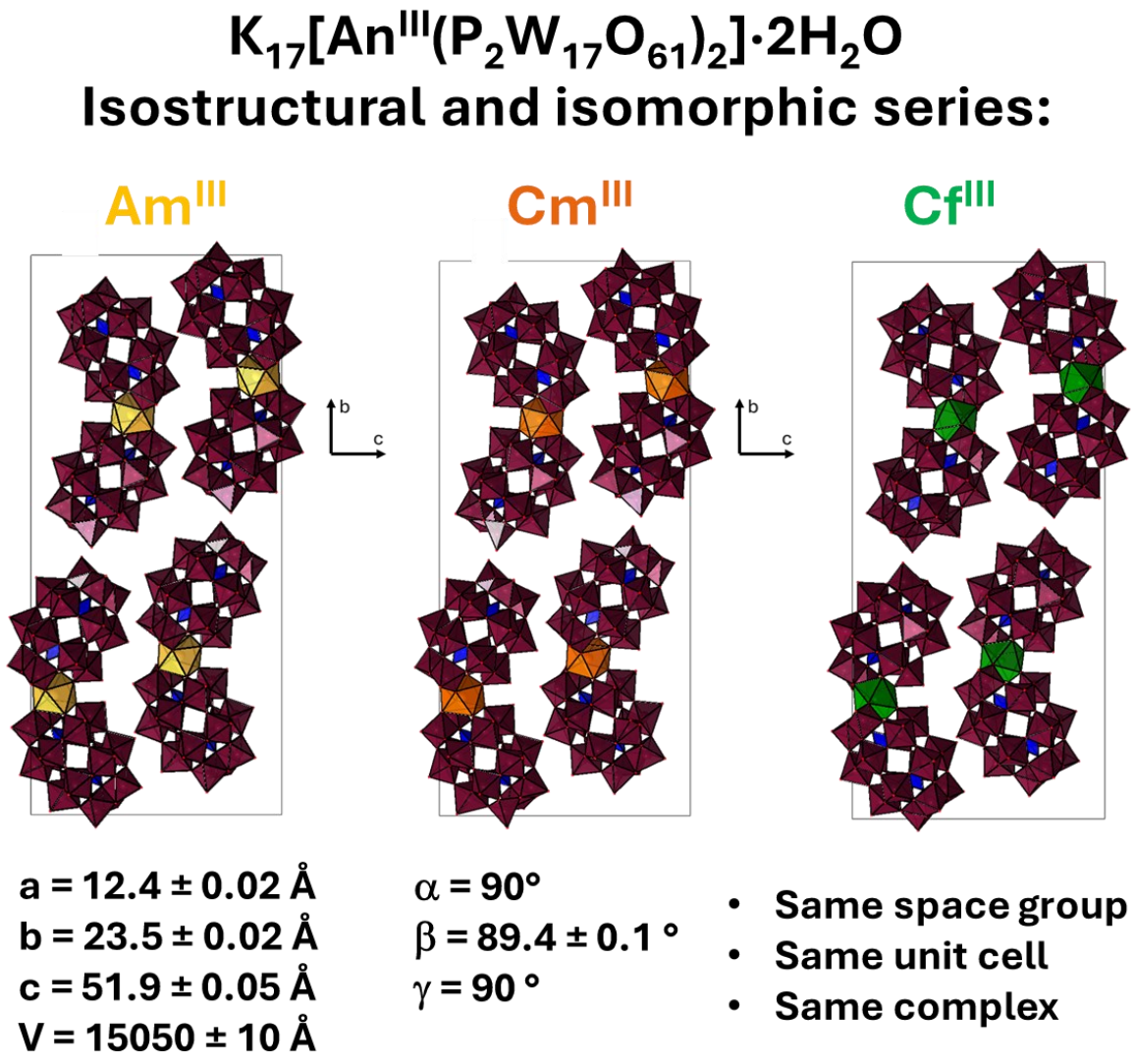

Figure S3. View of the isostructural and isomorphous compounds: $K_{17}Am(P_2W_{17}O_{61})_2 \cdot 12H_2O$, $K_{17}Cm(P_2W_{17}O_{61})_2 \cdot 8H_2O$, and $K_{17}Cf(P_2W_{17}O_{61})_2 \cdot 2H_2O$. See main text for more structural details.

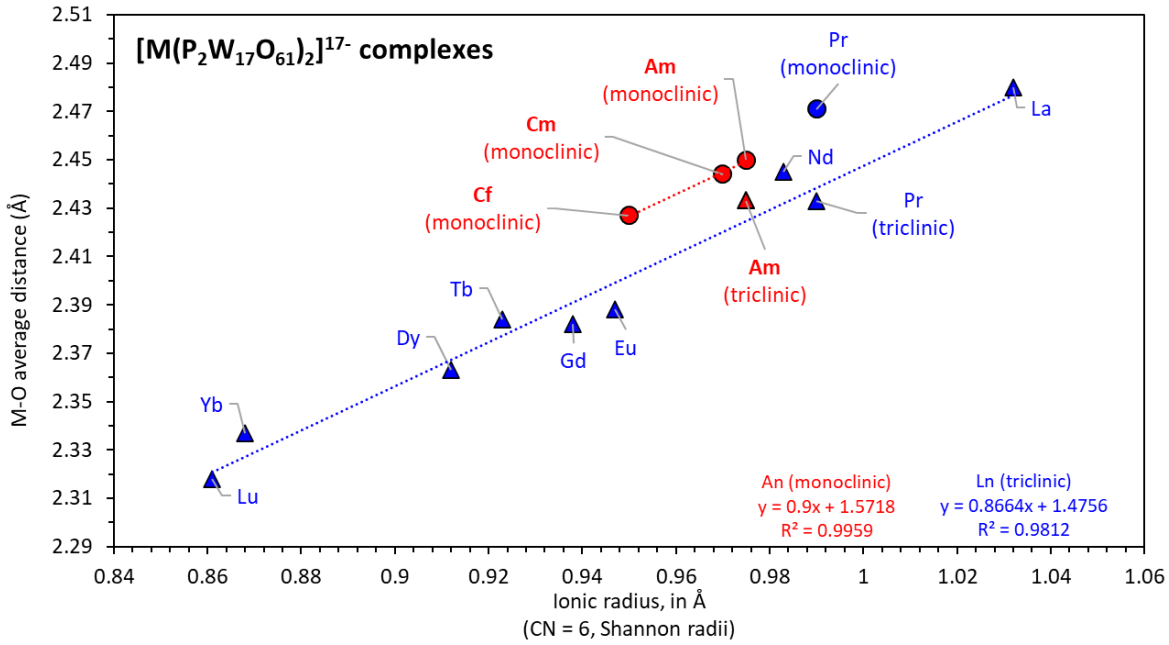

Figure S4. Correlation between the average metal-oxygen bond distance in $[M(P_2W_{17}O_{61})_2]^{17-}$ and the ionic radius of the f-element. Triangles: Triclinic phases. Circle: Monoclinic phases. The ionic radii used in this plot are from Shannon's list[14] , with a coordination number of 6 as this is the only list where all the metals studied here where available. $K_{17}Cf(P_2W_{17}O_{61})_2{\cdot}2H_2O$ (monoclinic) and $K_{17}Pr(P_2W_{17}O_{61})_2{\cdot}3H_2O$ (triclinic) are reported in the present study. See our companion paper[13] on $Am(P2W17)_2$ and $Cm(P2W17)_2$ for a compilation of the previously known structures with lanthanides and for crystallographic details on $K_{17}Nd(P_2W_{17}O_{61})_2{\cdot}4H_2O$ (triclinic), $K_{17}Pr(P_2W_{17}O_{61})_2$ (monoclinic), $K_{17}Am(P_2W_{17}O_{61})_2{\cdot}12H_2O$ (monoclinic), $K_{17}Am(P_2W_{17}O_{61})_2{\cdot}42.5H_2O$ (triclinic), and $K_{17}Cm(P_2W_{17}O_{61})_2{\cdot}8H_2O$ (monoclinic).

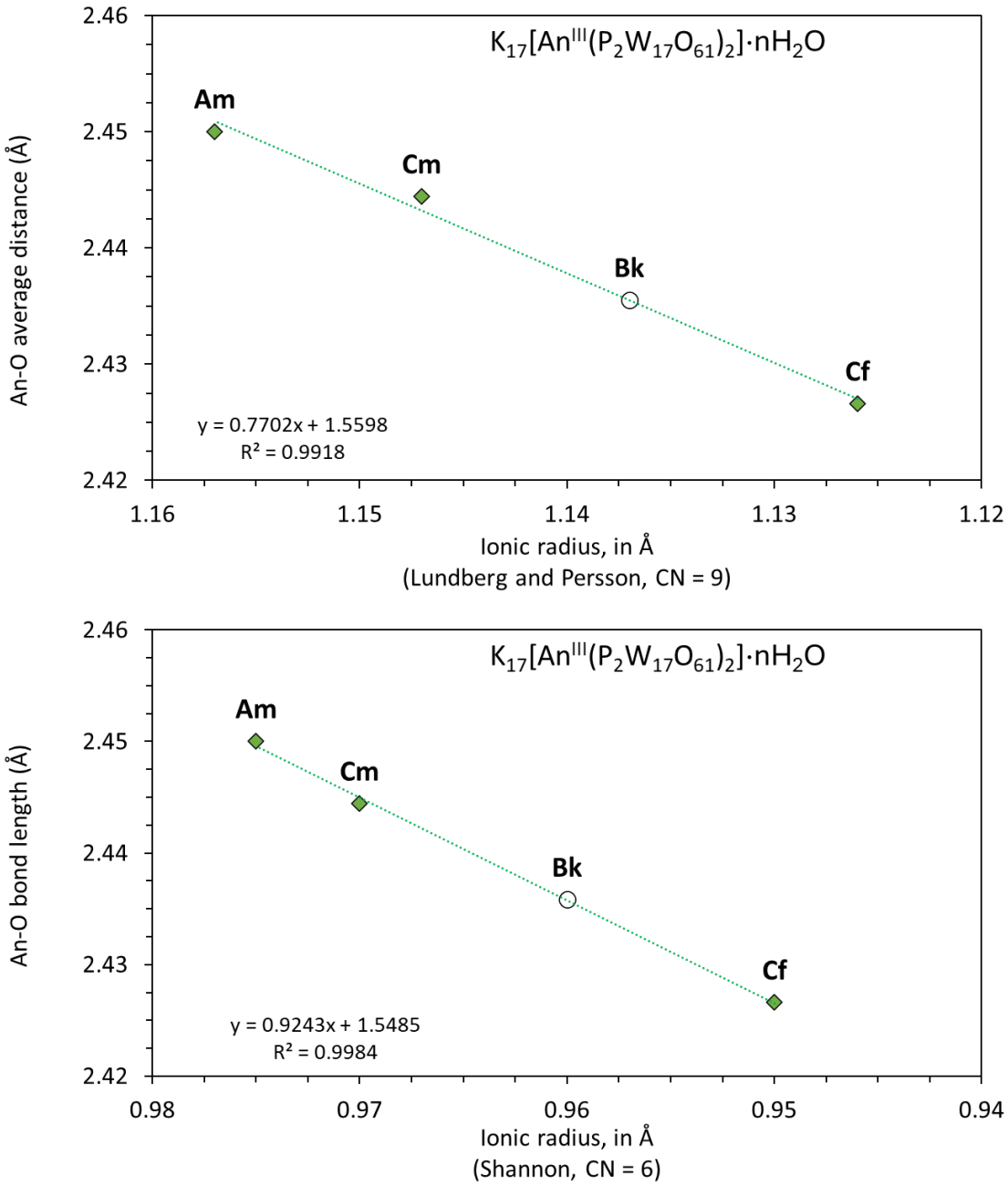

Figure S5. Correlation between the ionic radii of the actinide(III) and the observed bond distance in the $K_{17}Am(P_2W_{17}O_{61})_2 \cdot 12H_2O$, $K_{17}Cm(P_2W_{17}O_{61})_2 \cdot 8H_2O$, and $K_{17}Cf(P_2W_{17}O_{61})_2 \cdot 2H_2O$. Since there is no available experimental value for Cf^{3+} with a coordination number of 8, we used the ionic radii from Lundberg and Persson[15] (Coordination number of 9) and the ionic radii from Shannon[14] (Coordination number of 8). Both methods lead to the same extrapolated Bk^{III}-O bond distance: 2.436 Å.

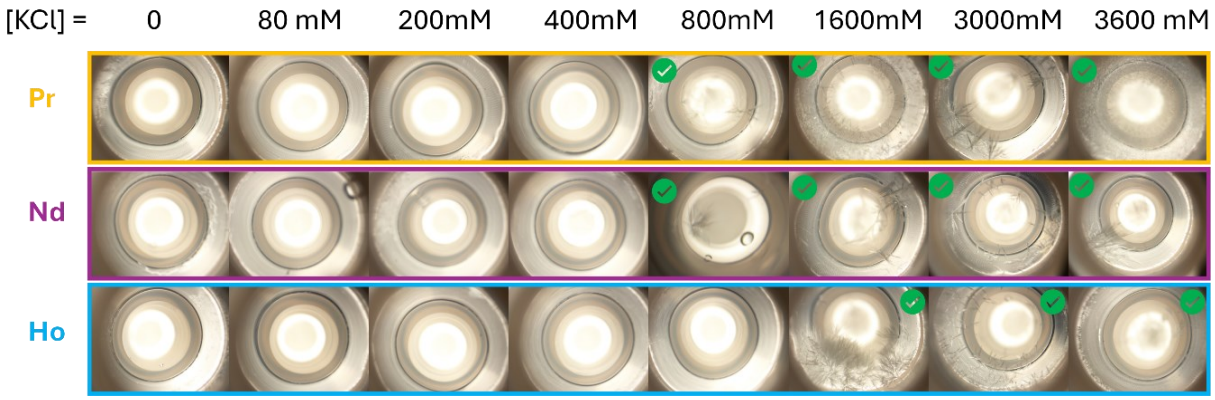

Figure S6. Crystallization tests with $Pr^{III}(P2W17)_2$, $Nd^{III}(P2W17)_2$, and $Ho^{III}(P2W17)_2$. [Ln] = 100 µM. [P2W17] = 200 µM. [KCl] = 0 to 3600 mM, as indicated above the pictures. Samples that yielded crystals are highlighted with a green tick mark.

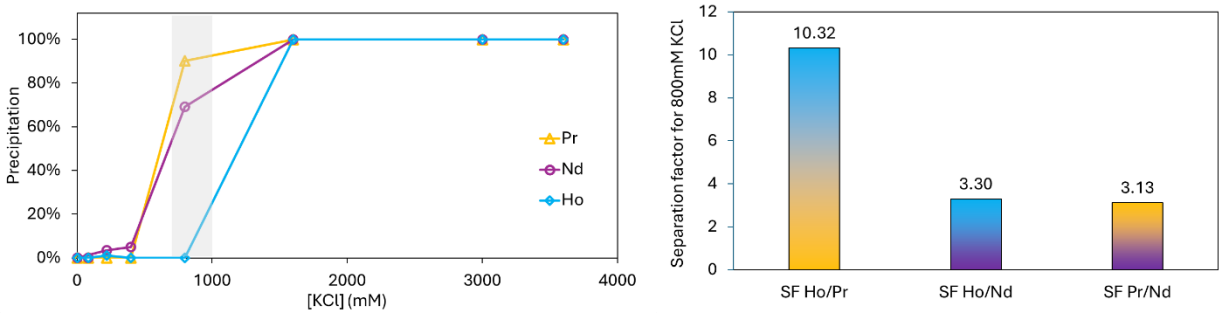

Figure S7. Precipitation yields corresponding to Figure S5 and calculated separation factors for the samples with 800 mM KCl.

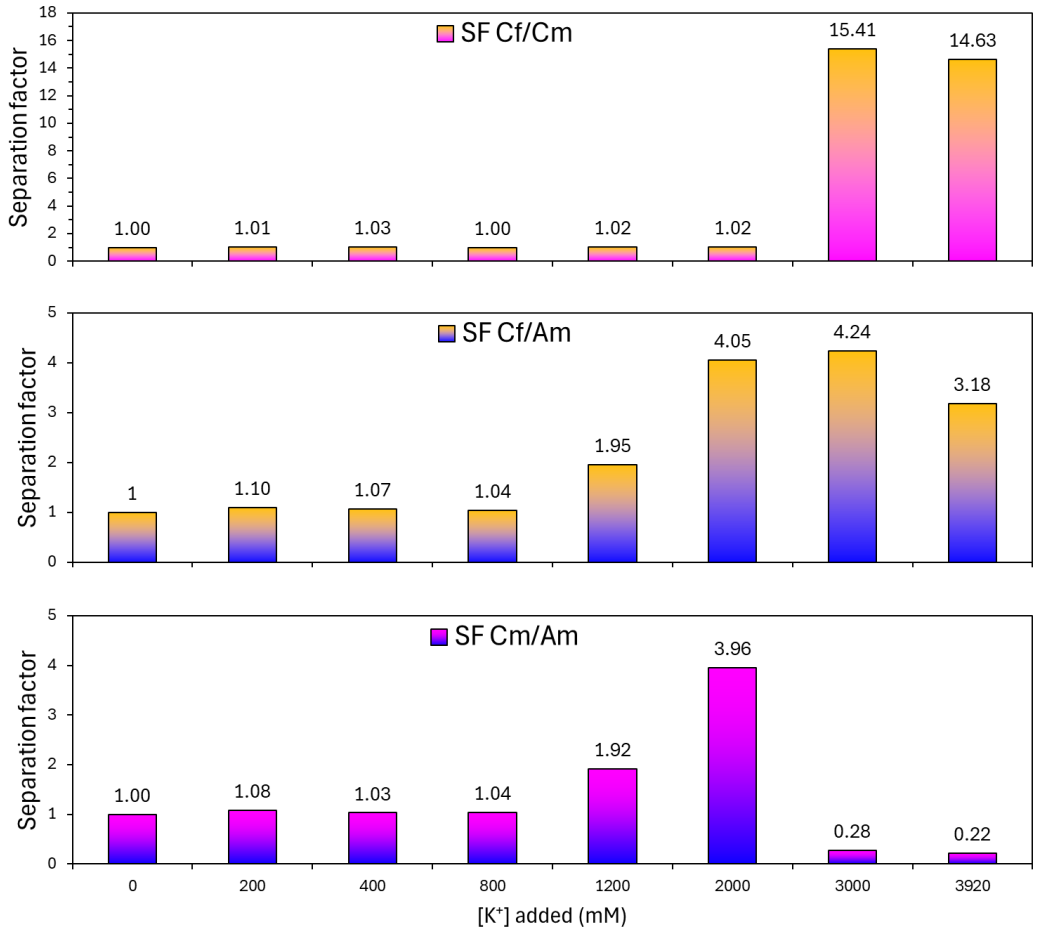

Figure S8. Calculated separation factors for $Am^{III}(P2W17)_2$, $Cm^{III}(P2W17)_2$, and $Cf^{III}(P2W17)_2$. [An] = 13 µM. [P2W17] = 27 µM. [KCl] = 0 to 3920 mM. See main text for more details. T = 22˚C. The equilibration time was 3 days. Similar or better results were obtained after 14 days (See Figure S9).

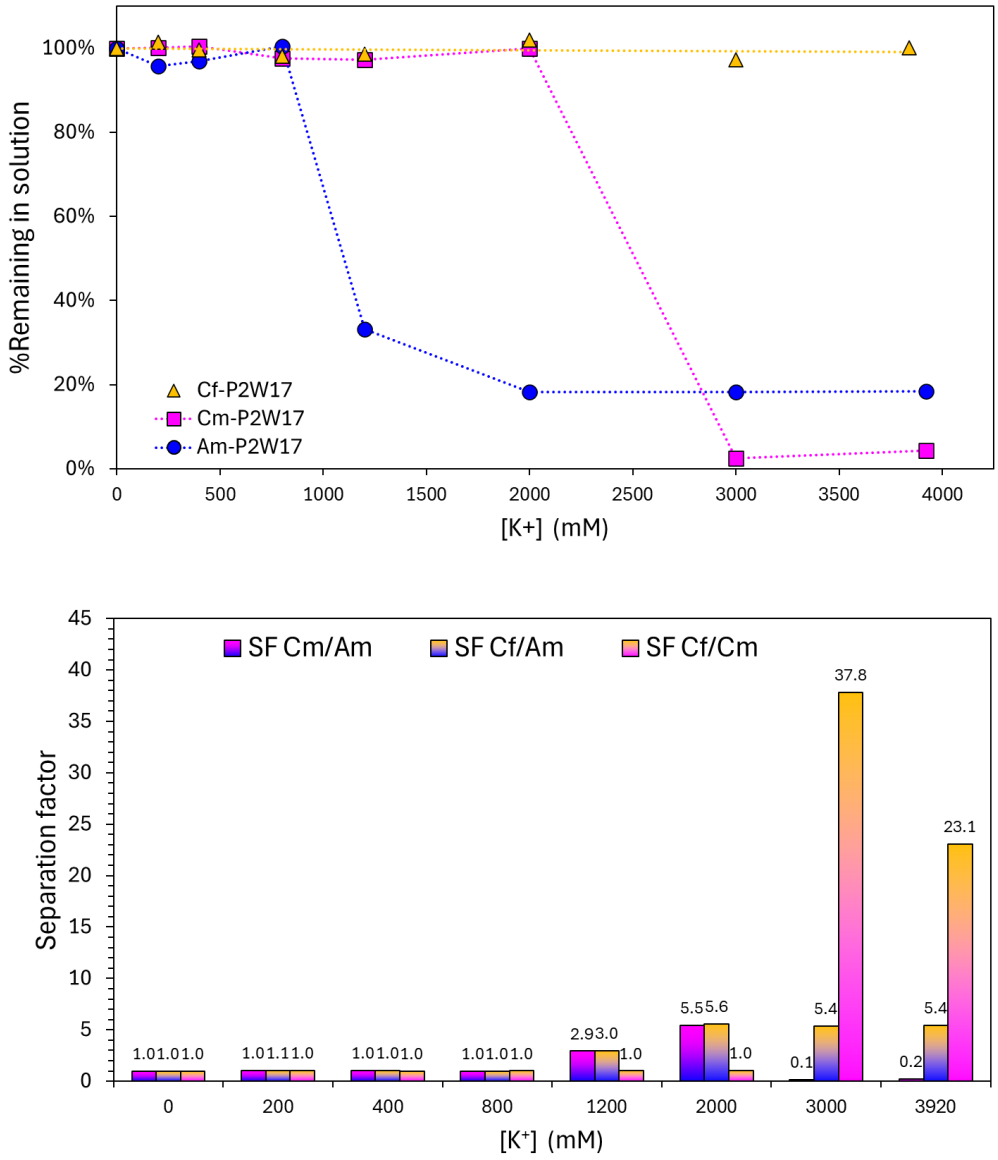

Figure S9. Calculated Solubility of $Am(P2W17)_2$, $Cm(P2W17)_2$, and $Cf(P2W17)_2$ at different concentrations of KCl and separation factors. See Fig. S8 for numerical values. T = 22˚C. Equilibration time = 14 days.

Experimental Section

Precaution: ^{249}Cf is highly radioactive and toxic! Extreme caution and appropriate procedures should be taken. All experiments involving radionuclides were conducted at Lawrence Livermore National Laboratory, in facilities designed for the safe handling of long-lived and short-lived radioactive materials and associated waste.

Materials: A californium source (^{249}Cf) was purchased from the NIDC (USA). $NaCH_3COO$ (≥99.9%), cesium chloride (>99.99%), $Na_2WO_4{\cdot}2H_2O$ (≥99%), phosphoric acid, potassium chloride and lanthanide trichloride salts (>99.9%) were purchased from chemical providers (VWR and Millipore Sigma) and used as received. All solutions were prepared using deionized water purified by reverse osmosis cartridge system (≥ 18.2 MΩ.cm). All experiments were performed in a temperature-controlled room (22°C).

Synthesis of $K_{10}P_2W_{17}O_{61}.20H_2O$. P_2W_{17} was prepared according to the synthesis reported by Randall et al.[16], by first isolating the $K_6P_2W_{18}O_{62}$ precursor. Thus, 8 g of the P_2W_{18} salt, prepared by the method of Contant et al. was dissolved in 20 ml water. To the P_2W_{18} aqueous solution, 2 g $HKCO_3$ was added and the mixture stirred for 1 h. Then, 10 g KCl was added to precipitate P_2W_{17}. The solid was filtered and dried under vacuum.

Synthesis of $K_{17}Cf(P_2W_{17}O_{61})_2{\cdot}2H_2O$. The $Cf^{III}(P2W17)_2$ complex was prepared in situ by directly mixing the stoichiometric amount of the POM and the actinides. The sample was buffered at pH 4.5 with 0.1 M sodium acetate. For crystallization, a 100 µL sample containing 20 µM of the complex (i.e., 500 nanograms of ^{249}Cf) was prepared. To this aqueous sample, 20 µL of saturated KCl solution was added. The sample was left closed and at room temperature. Contrary to its Am^{3+} and Cm^{3+} analogous compounds, no crystal appeared even after ~2 weeks. Given the apparently higher solubility of $Cf^{III}(P2W17)_2$ complex, it was left to evaporate very slowly over the course of another ~2 weeks, after which some crystals with a morphology reminiscent of the monoclinic $Am^{III}(P2W17)_2$ and $Cm^{III}(P2W17)_2$ compounds appeared (See Fig. S2). The best crystals were harvested from their mother liquor and mounted on crystallography pins for scXRD analysis. Presence of radioisotope in the mounted crystals was checked on the spot with radiological probes. Similar crystals were analyzed via solid-state UV-vis absorbance.

Solution-state UV-visible-NIR spectrophotometry. The solution-state absorbance spectrum of $Cf(P2W17)_2$ was measured using a high-performance Cary 6000i UV-vis-NIR spectrophotometer (Agilent Technologies). The sample was contained in a cuvette with a path length of 10 mm and was baseline corrected by measuring the absorbance of the corresponding buffer prior to measurement.

Solid-state UV-visible spectrophotometry. Absorbance spectra of the solid samples were measured using a CRAIC Technology 508 PV^{TM} microspectrophotometer. Crystals of $Cf(P2W17)_2$ were isolated from their mother liquor and the analysis was performed on multiple crystals to check for consistency. Crystals had the same crystal morphology and gave similar spectra. The spectral window was 400–900 nm as accessible by the white the light source of the instrument. The reported spectrum of $Cf(P2W17)_2$ is the averages of 200 scans, with an integration time per scan optimized by the instrument software for each sampling area.

Solubility and separation studies. Experiments were performed at 22˚C. Samples of $Am^{III}(P2W17)_2$, $Cm^{III}(P2W17)_2$ and $Cf^{III}(P2W17)_2$ were prepared in microcentrifuge tubes. Samples contained 13 μM of the actinide and 27 μM of the POM. The KCl concentration was varied from 0 to 3920 mM. Crystal formation appeared to be complete after ~2 days. Samples were left to equilibrate for 3 days before analysis (See Figure 4 in main text and Figures S7-S8). Samples were also reanalyzed after 14 days and gave similar or better results (Figure S9). For $Am^{III}(P2W17)_2$, formation of crystals was observed in the four highest KCl concentrations tested (1200, 2000, 3000, and 3920 mM). For $Cm^{III}(P2W17)_2$, formation of crystals was only observed in the two highest KCl concentrations tested (3000 and 3920 mM). For $Cf^{III}(P2W17)_2$ no crystal appeared in any of the samples. Concentrations of the actinide remaining in solution at chemical equilibrium were determined via liquid scintillation counting at secular equilibrium. Similar tests with lanthanides (Fig. S6-S7) where performed at a concentration of 100 μM and the lanthanide precipitation was tracked with UV-vis absorbance measurements.

Given the formula of the compounds derived from the single crystal structures, the solubility product is as follows:

$17\ K^+ + [M(P_2W_{17}O_{61})_2]^{17-} + n\ H_2O = K_{17}[M(P_2W_{17}O_{61})_2]\cdot nH_2O_{(s)}$

With $M = Ln^{3+}$ or An^{3+}.

Crystallographic studies. All structures were collected at LLNL's radiochemistry laboratories using a Rigaku Synergy Custom single crystal diffractometer, equipped with a kappa goniometer and using Mo Kα radiation (λ = 0.71073 Å) with a FWHM of ~200 μm at the sample from a MicroMax-007 HF microfocus rotating anode source. Images were recorded on a Dectris Pilatus 3R (300K – CdTe) detector and processed using CrysAlis^{Pro}. After integration both analytical absorption and empirical absorption (spherical harmonic, image scaling, detector scaling) corrections were applied.[17] All structures were solved by Intrinsic Phasing method from SHELXT program[18], developed by successive difference Fourier syntheses, and refined by full-matrix least square on all F^2 data using SHELX[19] via OLEX2 interface.[20]

Crystallographic information for the six reported structures can be obtained free of charge from the Cambridge Crystallographic Data Center (https://www.ccdc.cam.ac.uk/) upon referencing CCDC numbers in the crystallographic tables below.

Notes on crystal structures, refinement, modeling of disorder, and solvent void space. Due to safety protocols any californium containing crystals were collected under the MicroRT Capillaries 37mm. Although x-ray transparent at certain angles the background intensity increased resulting in poor signal-to-noise ratio, resulting in the use of some restraints.

Absorption correction was performed using Empirical absorption correction applied before frame scaling. Several other methods were employed, such as numerical absorption with a Gaussian grid (based on the crystal system), or analytical absorption correction after the Clark and Reid method before ultimately using a combination of Gaussian grid absorption correction and "Mutli-scan" using the Scale3 Abspack.[3] All of these methods relied on measuring the face of the crystal using CCD images capture before collection. The resulting R_{int} after absorption correction dropped for each structure by approximately 3%. Nevertheless, large residual electron density less than 1 Å away from the tungsten atoms remained.

Furthermore, individual hydrogen atoms could not be refined, as such they have been omitted in the reported molecular weight.

Common cif alerts and responses thereof

- **PLAT971/2/3_ALERT_2_A Check Calcd Resid. Dens. X Ang from X**

Response: High residual Q-peaks of 0.1*Z/Å^3 at 0.6 – 1.2 Å away from the heavy atoms (15). While most structures are within this range, we nevertheless processed the data through

several different absorption correction methods before ultimately using spherical or multi-scan methods. (15)

- **PLAT910_ALERT_3_B Missing # of FCF Reflection(s) Below Theta(Min).**
  Response: Missing hkl reflection missing due to beam stop mask applied to detector during data collection while at minimal distance allowed by the instrument. As such, a decision was taken to sacrifice a few reflections for higher overall intensity, due to the size and synthesis nature of the crystals.

- **PLAT306_ALERT_2_B Isolated Oxygen Atom (H-atoms Missing ?)**
  Response: solvent water molecules, H-atoms not located.
  Individual cases are discussed below.

References:

1 R. E. Sykora, Z. Assefa, R. G. Haire and T. E. Albrecht-Schmitt, *Inorg. Chem.*, 2006, **45**, 475–477.
2 C. Apostolidis, B. Schimmelpfennig, N. Magnani, P. Lindqvist-Reis, O. Walter, R. Sykora, A. Morgenstern, E. Colineau, R. Caciuffo, R. Klenze, R. G. Haire, J. Rebizant, F. Bruchertseifer and T. Fanghänel, *Angewandte Chemie International Edition*, 2010, **49**, 6343–6347.
3 M. J. Polinski, E. B. Garner, R. Maurice, N. Planas, J. T. Stritzinger, T. G. Parker, J. N. Cross, T. D. Green, E. V. Alekseev, S. M. V. Cleve, W. Depmeier, L. Gagliardi, M. Shatruk, K. L. Knappenberger, G. Liu, S. Skanthakumar, L. Soderholm, D. A. Dixon and T. E. Albrecht-Schmitt, *Nature Chem*, 2014, **6**, 387–392.
4 S. K. Cary, M. Vasiliu, R. E. Baumbach, J. T. Stritzinger, T. D. Green, K. Diefenbach, J. N. Cross, K. L. Knappenberger, G. Liu, M. A. Silver, A. E. DePrince, M. J. Polinski, S. M. V. Cleve, J. H. House, N. Kikugawa, A. Gallagher, A. A. Arico, D. A. Dixon and T. E. Albrecht-Schmitt, *Nat Commun*, 2015, **6**, 1–8.
5 S. K. Cary, J. Su, S. S. Galley, T. E. Albrecht-Schmitt, E. R. Batista, M. G. Ferrier, S. A. Kozimor, V. Mocko, B. L. Scott, C. E. Van Alstine, F. D. White and P. Yang, *Dalton Trans.*, 2018, **47**, 14452–14461.
6 S. S. Galley, S. A. Pattenaude, C. A. Gaggioli, Y. Qiao, J. M. Sperling, M. Zeller, S. Pakhira, J. L. Mendoza-Cortes, E. J. Schelter, T. E. Albrecht-Schmitt, L. Gagliardi and S. C. Bart, *J. Am. Chem. Soc.*, 2019, **141**, 2356–2366.
7 J. M. Sperling, E. Warzecha, C. J. Windorff, B. E. Klamm, A. N. Gaiser, M. A. Whitefoot, F. D. White, T. N. Poe and T. E. Albrecht-Schönzart, *Inorg. Chem.*, 2020, **59**, 10794–10801.
8 N. Brenner, J. M. Sperling, T. N. Poe, C. Celis-Barros, K. Brittain, E. M. Villa, T. E. Albrecht-Schmitt and M. J. Polinski, *Inorg. Chem.*, 2020, **59**, 9384–9395.
9 C. A. P. Goodwin, J. Su, L. M. Stevens, F. D. White, N. H. Anderson, J. D. Auxier, T. E. Albrecht-Schönzart, E. R. Batista, S. F. Briscoe, J. N. Cross, W. J. Evans, A. N. Gaiser, A. J. Gaunt, M. R. James, M. T. Janicke, T. F. Jenkins, Z. R. Jones, S. A. Kozimor, B. L. Scott, J.

M. Sperling, J. C. Wedal, C. J. Windorff, P. Yang and J. W. Ziller, *Nature*, 2021, **599**, 421–424.
10 T. N. Poe, H. Ramanantoanina, J. M. Sperling, H. B. Wineinger, B. M. Rotermund, J. Brannon, Z. Bai, B. Scheibe, N. Beck, B. N. Long, S. Justiniano, T. E. Albrecht-Schönzart and C. Celis-Barros, *Nat. Chem.*, 2023, **15**, 722–728.
11 Z. Bai, N. B. Beck, B. Scheibe, J. M. Sperling, A. Weiland, M. Ruf, J. P. Brannon, B. M. Rotermund, D. Gomez Martinez and T. E. Albrecht-Schönzart, *J. Am. Chem. Soc.*, 2024, **146**, 7822–7830.
12 V. R. M. Nielsen and T. Just Sørensen, *Nat Commun*, 2025, **16**, 11122.
13 I. Colliard and G. Deblonde, 2025, preprint.
14 R. D. Shannon, *Acta crystallographica*, 1976, **A32**, 751–767.
15 D. Lundberg and I. Persson, *Coordination Chemistry Reviews*, 2016, **318**, 131–134.
16 W. J. RANDALL, D. K. LYON, P. J. DOMAILLE and R. G. FINKE, in *Inorganic Syntheses*, John Wiely & Sons, Inc, 1998, vol. 32, pp. 242–268.
17 G. M. Sheldrick, Bruker-Siemens area Detection Absorption other Correction (version 2008/12008) 2008.
18 G. M. Sheldrick, *Acta Cryst A*, 2015, **71**, 3–8.
19 G. M. Sheldrick, *Acta Cryst A*, 2008, **64**, 112–122.
20 O. V. Dolomanov, L. J. Bourhis, R. J. Gildea, J. a. K. Howard and H. Puschmann, *J Appl Cryst*, 2009, **42**, 339–341.